Thermodynamic properties and electrical conductivity of strongly correlated plasma media



2009 J. Phys. A: Math. Theor. 42 214002

(http://iopscience.iop.org/1751-8121/42/21/214002)

IOP PUBLISHING JOURNAL OF PHYSICS A: MATHEMATICAL AND THEORETICAL

J. Phys. A: Math. Theor. **42** (2009) 214002 (9pp) doi:10.1088/1751-8113/42/21/214002

# Thermodynamic properties and electrical conductivity of strongly correlated plasma media

**V S Filinov[1], P R Levashov[1], A V Boţan[1], M Bonitz[2] and V E Fortov[1]**

[1] Joint Institute for High Temperatures, Russian Academy of Sciences, Izhorskaya 13 bldg 2, Moscow 125412, Russia
[2] Christian-Albrechts-Universität zu Kiel, Institut für Theoretische Physik und Astrophysik, Leibnizstrasse 15, 24098 Kiel, Germany

Received 14 October 2008, in final form 15 January 2009
Published 8 May 2009
Online at stacks.iop.org/JPhysA/42/214002

**Abstract**
We study thermodynamic properties and the electrical conductivity of dense hydrogen and deuterium using three methods: classical reactive Monte Carlo, direct path integral Monte Carlo (PIMC) and a quantum dynamics method in the Wigner representation of quantum mechanics. We report the calculation of the deuterium compression quasi-isentrope in good agreement with experiments. We also solve the Wigner–Liouville equation of dense degenerate hydrogen calculating the initial equilibrium state by the PIMC method. The obtained particle trajectories determine the momentum–momentum correlation functions and the electrical conductivity and are compared with available theories and simulations.

PACS numbers: 52.65.Pp, 52.25.Kn, 52.25.Fi

## 1. Introduction

During the last decades significant efforts have been made to investigate the thermophysical properties of dense hydrogen and deuterium [1–5]. The importance of this activity is mainly connected with the creation of new experimental facilities. Powerful current generators [2] and ultrashort lasers [3] are used to produce very high pressures which cannot be reached in traditional explosive devices and light-gas guns. Such experiments give valuable information about various properties of strongly coupled plasmas. This allows one to obtain a wide-range equation of state, e.g. [6–8], and to verify various theoretical approaches [9, 11] and numerical methods [12, 13].

As a result of the development of modern supercomputers molecular simulation such as classical molecular dynamics (MD) and Monte Carlo (MC) became a traditional way of calculating thermodynamic and transport properties of non-ideal plasma, e.g. [14–16]. The main difficulty, however, remains the treatment of bound states in a dense plasma environment.

  

As this is a quantum-mechanical or quantum-statistical problem more complex simulation approaches are required such as density functional theory (DFT) or path integral MC (PIMC). In these '*ab initio*' methods however, one needs to employ some criterion to identify a bound state [17, 18]. This is the reason why classical methods with a quantum-mechanical treatment of bound states are frequently used together with first-principle ones.

The dynamical electrical conductivity is of fundamental importance for the plasma behavior in a high-frequency electromagnetic field, in particular for the interaction of charged particles with intense radiation and for inertial thermonuclear fusion. There are many theoretical models of dynamic conductivity which can be derived from a kinetic theory [9–11]. Molecular simulations of fully ionized classical plasma are widely used for the calculation of electrical conductivity with the help of the Kubo formula [11], but our main interest is to improve these results by taking into account bound states and quantum exchange-correlation effects. This can be done by means of DFT theory, but it treats exchange-correlation effects approximately and cannot be applied at high temperatures. PIMC, on the other hand, is free from these drawbacks and therefore can be used for the construction of a generalized molecular dynamics method for the calculation of electrical conductivity.

## 2. Simulation methods

Here we describe the computational methods which have been used for the calculation of thermodynamic properties and electrical conductivity of dense hydrogen and deuterium.

### *2.1. Thermodynamic properties*

Thermodynamics is calculated by two approaches: the reaction MC (REMC) method [19, 20] and the PIMC approach [14, 22]. The main attention is paid to the region of the hypothetical plasma phase transition (PPT). We also perform a comparison with recent experimental results on the quasi-isentropic compression of deuterium [37].

A complete description of the REMC method can be found in [19, 20]. Here we consider only molecular hydrogen dissociation and recombination: $H_2 \Leftrightarrow 2H$. Ionization can be neglected at temperatures lower than the hydrogen ground-state energy ($\propto$13.6 eV) and at moderate densities; at significant ionization degrees PIMC is used. The effective pair potentials between different particle species are approximated by the Buckingham-EXP6 potentials, corrected at small distances [7]. Our REMC simulations have been performed in the canonical ensemble for hydrogen and deuterium. We use three types of MC moves: particle displacement, molecular dissociation into atoms and recombination to a molecule. The expressions for probabilities of the two last moves are given by the internal partition functions of atoms and molecules $Z_A^{\rm int}$, $Z_M^{\rm int}$. All electrons (in atoms and molecules) are assumed to be in the ground state. Further, $Z_A^{\rm int}$ contains only translational degrees of freedom, $Z_M^{\rm int}$ contains, in addition, rotational and vibrational degrees of freedom. For the latter we numerically solve the Schrödinger equation in a central-symmetric field, as described in [21], which yields the energy levels $E_{nl}$.

The PIMC method allows for first-principle simulations of dense plasmas at arbitrary coupling and up to moderate degeneracy parameters, for details on our method, see [14, 22]. It has been used for calculation of thermodynamic properties of hydrogen and hydrogen–helium plasmas and electron–hole plasma in semiconductors [18, 27–29]. Details about simulation by both REMC and PIMC methods will be given in section 3.1.

### *2.2. Electrical conductivity*

To calculate the electrical conductivity we use quantum dynamics (QMD) in the Wigner representation of quantum mechanics. The Wigner–Liouville equation is solved by a combination of MD and MC methods. The initial conditions are obtained using PIMC which yields thermodynamic quantities such as the internal energy, pressure and pair distribution functions in a wide range of density and temperature. To study the influence of the Coulomb interaction on the dynamic properties of dense plasmas we apply the quantum dynamics in the canonical ensemble at finite temperature and compute temporal momentum–momentum correlation functions and their frequency-domain Fourier transforms.

Below we briefly describe our QMD simulations of the conductivity. Our starting point is the canonical ensemble-averaged time correlation function [11]

$$C_{FA}(t) = \langle \hat{F}(0)\hat{A}(t)\rangle = Z^{-1}\mathrm{Tr}\{\hat{F}\,\mathrm{e}^{\mathrm{i}\hat{H}t_c^*/\hbar}\hat{A}\,\mathrm{e}^{-\mathrm{i}\hat{H}t_c/\hbar}\}, \tag{1}$$

where $\hat{F}$ and $\hat{A}$ are operators of arbitrary observables and $\hat{H}$ is the Hamiltonian of the system which is the sum of the kinetic $\hat{K}$ and the potential $\hat{U}$ energy operators and the complex time is $t_c = t - \mathrm{i}\hbar\beta/2$, and $\beta = 1/k_BT$. $Z = \mathrm{Tr}\{\mathrm{e}^{-\beta\hat{H}}\}$ is the partition function. The Wigner representation of (1) in a $\upsilon$-dimensional space is

$$C_{FA}(t) = (2\pi\hbar)^{-2\upsilon} \times \iint \mathrm{d}\mu_1\,\mathrm{d}\mu_2 F(\mu_1)A(\mu_2)W(\mu_1;\mu_2;t;\mathrm{i}\hbar\beta),$$

where $\mu_i = (p_i, q_i), (i = 1, 2)$, and $p$ and $q$ comprise the momenta and coordinates, respectively, of all particles. $A(\mu)$ and $F(\mu)$ denote the Weyl's symbols of the operators

$$A(\mu) = \int \mathrm{d}\xi\,\mathrm{e}^{-\mathrm{i}\frac{p\xi}{\hbar}}\left\langle q - \frac{\xi}{2}\middle|\hat{A}\middle|q + \frac{\xi}{2}\right\rangle$$

and $W(\mu_1;\mu_2;t;\mathrm{i}\hbar\beta)$ is the spectral density expressed as

$$W(\mu_1;\mu_2;t;\mathrm{i}\hbar\beta) = \frac{1}{Z}\iint \mathrm{d}\xi_1\,\mathrm{d}\xi_2\,\mathrm{e}^{\mathrm{i}\frac{p_1\xi_1}{\hbar}}\,\mathrm{e}^{\mathrm{i}\frac{p_2\xi_2}{\hbar}} \times\left\langle q_1 + \frac{\xi_1}{2}\middle|\,\mathrm{e}^{\mathrm{i}\hat{H}t_c^*/\hbar}\middle|q_2 - \frac{\xi_2}{2}\right\rangle\left\langle q_2 + \frac{\xi_2}{2}\middle|\,\mathrm{e}^{-\mathrm{i}\hat{H}t_c/\hbar}\middle|q_1 - \frac{\xi_1}{2}\right\rangle.$$

As has been proved in [24, 25], $W$ obeys the following integral equation:

$$\begin{aligned} W(\mu_1;\mu_2;t;\mathrm{i}\hbar\beta) &= \bar{W}(\bar{p}_0,\bar{q}_0;\tilde{p}_0,\tilde{q}_0;\mathrm{i}\hbar\beta) \\ &+ \frac{1}{2}\int_0^t \mathrm{d}\tau \int \mathrm{d}s\,W(\bar{p}_\tau - s,\bar{q}_\tau;\tilde{p}_\tau,\tilde{q}_\tau;\tau;\mathrm{i}\hbar\beta)\varpi(s,\bar{q}_\tau) \\ &- \frac{1}{2}\int_0^t \mathrm{d}\tau \int \mathrm{d}s\,W(\bar{p}_\tau,\bar{q}_\tau;\tilde{p}_\tau - s,\tilde{q}_\tau;\tau;\mathrm{i}\hbar\beta)\varpi(s,\tilde{q}_\tau), \end{aligned} \tag{2}$$

where $\bar{W}(\bar{p}_0,\bar{q}_0;\tilde{p}_0,\tilde{q}_0;\mathrm{i}\hbar\beta)$ is the initial condition of equation (2), which can be presented in the form of a finite difference approximation of the Feynman path integral [24, 25]. The expression for $W$ has to be generalized to account for spin effects giving rise to an additional spin part of the initial density matrix, e.g. [22]. Also, to improve the simulation accuracy the pair interactions $U_{ab}$, are replaced by an effective quantum potential $U_{ab}^{\mathrm{eff}}$, such as the Kelbg potential [26]. For details we refer to [14, 22], for recent applications of the PIMC approach to correlated Coulomb systems, cf [27–29].

The solution of the integral equation (2) can be represented by an iteration series

$$W^t = \bar{W}^t + K_\tau^t W^\tau = \bar{W}^t + K_{\tau_1}^t \bar{W}^{\tau_1} + \cdots,$$

where $\bar{W}^t$ and $\bar{W}^{\tau_1}$ are the initial quantum spectral densities evolving classically during time intervals $[0, t]$ and $[0, \tau_1]$, respectively, whereas $K_{\tau_i}^{\tau_{i+1}}$ are operators that govern the propagation from time $\tau_i$ to $\tau_{i+1}$, see e.g. [30]. Thus the time correlation function becomes

$$C_{FA}(t) = (\phi|W^t) = (\phi|\bar{W}^t) + \left(\phi|K_{\tau_1}^t \bar{W}^{\tau_1}\right) + \cdots,$$

where $\phi(\mu_1; \mu_2) \equiv F(\mu_1)A(\mu_2)$ and the parentheses $(\cdots|\cdots)$ denote integration over the phase space $\{\mu_1; \mu_2\}$. To compute the electrical conductivity we calculate the momentum–momentum time correlation function $C_{pp}(t)$ and then apply the Kubo formula which contains the Fourier transform of $C_{pp}(t)$.

The iteration series for $C_{FA}(t)$ can efficiently be computed using MC methods. We have developed a MC scheme which provides a domain sampling of the terms giving the main contribution to the iteration series, cf [24, 25]. For simplicity, in this work, we take into account only the first term of iteration series, which is related to the propagation of the initial quantum distribution $\bar{W}$ according to the Hamiltonian equations of motion. This term, however, is not a classical solution of equation (2) but accounts for quantum effects [31] and, in fact, contains arbitrarily high powers of the Planck's constant.

## 3. Numerical results

### *3.1. Deuterium compression isentrope*

To calculate an isentrope one has to determine the entropy which is defined by $S = -[\partial F(T, V, N)/\partial T]_V$, where $F = \sum_{i=1}^{2} N_i\mu_i - PV$ is the free energy of a two-component system of atoms and molecules. The chemical potentials $\mu_i$ of each component are obtained with the test particle method [32]: $\mu = \mu^{id} + \mu^r$, where $\mu^{id}$ is the ideal gas chemical potential: $\mu^{id} = k_B T \ln(\Lambda^3 N/V)$ and $\Lambda$ is the de Broglie wavelength of a particle. The residual chemical potential $\mu^r$ can be evaluated as [33]

$$\mu^r = -k_B T \ln[L_a \exp(-\Delta U/k_B T)].$$

Here $\Delta U$ denotes the change of configurational energy produced by the insertion of one additional particle and $L_a$ is the ratio of allowed (nonoverlapped) insertion intervals along trajectories which traverse (parallel to any of the axes) the simulation box from side-to-side to the length of the box [33]. The test particle is then inserted randomly into some point in the allowed intervals and the change in configurational energy $\Delta U$ is evaluated. The main advantage of this approach is the possibility of calculation of chemical potentials at high densities, where the usual test particle method tends to fail. The chemical potentials are calculated separately for atoms and molecules.

The isentrope can also be calculated by using the Zel'dovich's method [34, 35]. From the first law of thermodynamics the characteristic equation for the temperature along the isentrope can be derived,

$$\frac{\mathrm{d}T}{\mathrm{d}V} = -\frac{T}{(\partial E/\partial P)_V}.$$

We integrate this equation with the initial condition corresponding to an experimental point at low pressure taking the temperature at this point to be close to that from the Widom's test particle method. The coefficient $(\partial E/\partial P)_V$ is obtained from the interpolation functions $E(T, V)$ and $P(T, V)$, which are constructed from the REMC calculation on the grid of isotherms and isochores covering the experimental isentrope. Calculations were performed in a cubic simulation box with periodic boundary conditions, and with a cutoff radius equal to half of the box length. The initial particle configuration was an fcc lattice for every input

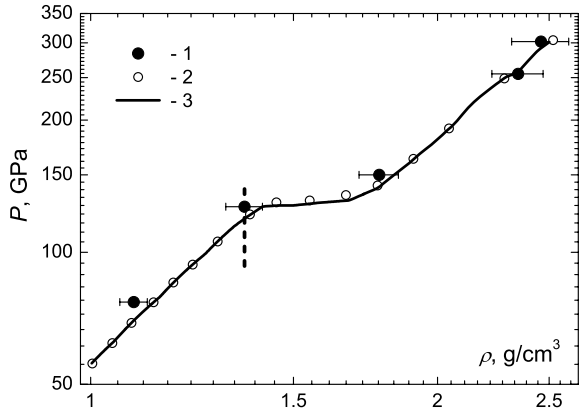


**Figure 1.** Deuterium quasi-isentropic compression. Experiment: 1—[37]. This work: 2—Widom's test particle method, 3—Zel'dovich's method. The vertical line shows the density at which a sharp electrical conductivity rise is observed in the experiment of [1, 40].

density $\rho = N_{\mathrm{H}} m_{\mathrm{H}}/V + N_{\mathrm{H}_2} m_{\mathrm{H}_2}/V$ with $N_{\mathrm{H}} = N_{\mathrm{H}_2} = 250$. The system was equilibrated for $2 \times 10^7$ steps, and an additional $10^7$ steps were used for the calculation of thermodynamic values. Averaging of 20 blocks was used to calculate the statistical error, which did not exceed 2% for pressure and energy.

In the PIMC method we used 50 protons (deuterons) and 50 electrons in a cubic cell with periodic boundary conditions and $20, \ldots, 40$ multipliers in the path integral representation of the density matrix. The number of configurations in the simulations was chosen such that the statistical error did not exceed 5%.

The results for three shock Hugoniots of gaseous deuterium with three different initial densities ($\rho_0 = 0.1335$ g cm$^{-3}$, $P_0 = 1.57$ GPa; $\rho_0 = 0.153$ g cm$^{-3}$, $P_0 = 2.03$ GPa; $\rho_0 = 0.171$ g cm$^{-3}$, $P_0 = 2.72$ GPa) obtained by REMC and PIMC methods can be found elsewhere [36]. Here we present our recent simulations of deuterium quasi-isentrope of compression. A dramatic increase of conductivity of deuterium by 4–5 orders of magnitude [1] at pressures ∼1 Mbar and densities about 1 g cm$^{-3}$ indicates that one might also expect peculiarities in the thermodynamic properties. Indeed, there are experimental results on quasi-isentropic compression of deuterium in a cylindrical explosive chamber which show a 30% density jump at a pressure of about 1.4 Mbar [37]. Using Zel'dovich's and Widom's test particle methods we calculated the compression isentrope of deuterium. The results are shown in figure 1 and compared to experimental data [37]. The excellent agreement between two isentrope reconstruction methods and the experiment proves that no special assumptions about a phase transition are needed to explain such a remarkable behavior of the experimental points, apparently dissociation effects mostly contribute to this phenomenon.

A comparison of our results with other theoretical and computational methods is shown in the phase diagram, figure 2. The temperature and density jump along the isentrope is close to the predicted boundary of the deuterium phase transition from the molecular to the atomic phase [12, 38, 39]. The rectangle shows the region of slow convergence of the simulations to the equilibrium state which might be an indication of a thermodynamic instability. Our preliminary analysis shows that this state can be stable (up to $\approx 2 \times 10^9$ Monte Carlo steps are required), but to investigate the possibility of phase separation at these conditions one needs to apply special MC methods which work in the grand canonical or Gibbs ensembles.

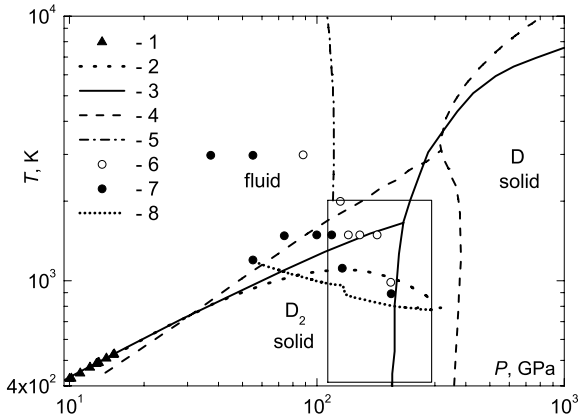


**Figure 2.** Deuterium phase diagram. Melting curve: 1—experiment [42]; 2—extrapolation of experiment [42]. Theoretical phase diagram: 3—[43]; 4—[41]. Boundary of the possible phase transition: 5—[38]. Atomic fluid: 6—[12, 39]. Molecular liquid: 7—[12, 39]. This work: 8—isentrope; the black rectangle shows the region of slow convergence to the equilibrium state.

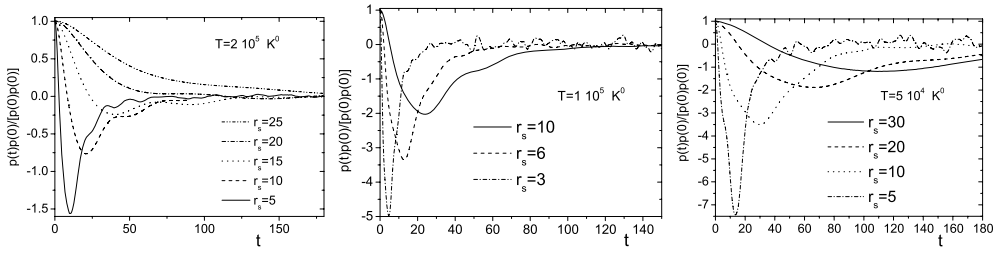


**Figure 3.** Typical MMCF in the canonical ensemble for different densities and three temperatures: $T = 200\,000$ K (left, $\Gamma = 0.3$, $\chi = 0.06$ at $r_s = 5$), $T = 100\,000$ K (center, $\Gamma = 1.0$, $\chi = 0.8$ at $r_s = 3$) and $T = 50\,000$ K (right, $\Gamma = 1.3$, $\chi = 0.5$ at $r_s = 5$). Time is given in atomic units.

### *3.2. Quantum momentum–momentum correlation functions*

We now compute the dynamical conductivity of a strongly coupled hydrogen plasma. The simulation results were practically insensitive to the variation of the whole particle number in the MC box from 30 up to 60 and also to the number $n$ of high-temperature density matrices in the path integral representation of the initial state (we used $n = 20$–$40$). Estimates of the average statistical error gave a value of the order 5–7%. According to the Kubo formula [11] our calculations include two stages: (i) generation of the initial conditions (configuration of protons and electrons) in the canonical ensemble with the probability being proportional to the quantum density matrix and (ii) generation of the dynamic trajectories in phase space, starting from these initial configurations.

First we discuss the momentum–momentum autocorrelation functions (MMCF) which are shown in figure 3 for various temperatures and densities. The plasma density is characterized by the Brueckner parameter $r_s = d/a_B$—the ratio of the mean interparticle distance $d$ to the Bohr radius where $d^{-3} = 4\pi(n_e + n_p)/3$ and $n_e$ and $n_p$ are the electron and proton densities. To estimate interaction and quantum effects we use the coupling parameter $\Gamma = e^2/(r_s a_B k_B T)$ and the degeneracy parameter $\chi = n_e \Lambda_e^3$ with $\Lambda_e$ being the electron thermal wavelength. The monotonic decay of the MMCF at low density transforms into aperiodic oscillations at high

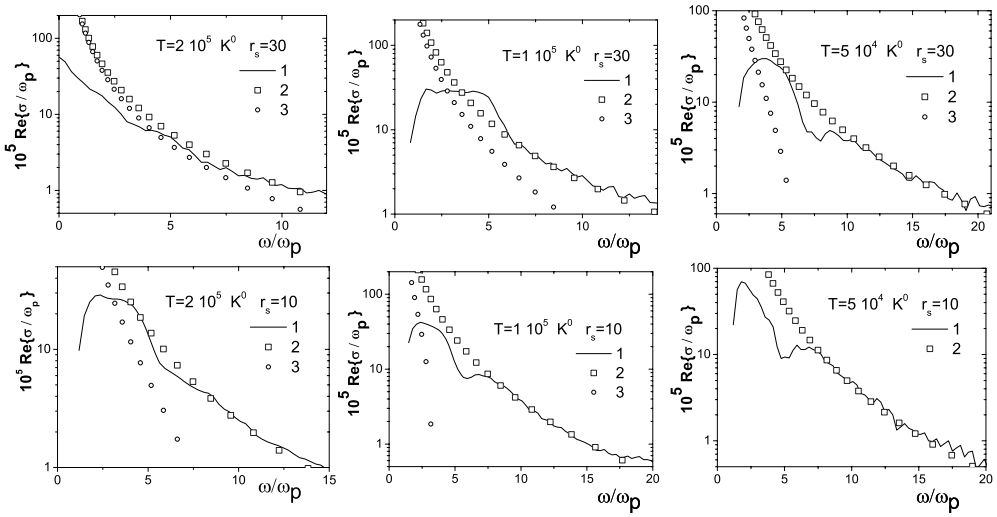


**Figure 4.** Real part of the Fourier transform of the MMCF (line 1) for densities related to three temperatures: $T = 200\,000$ K (left column, $\Gamma = 0.2$, $\chi = 0.007$), $T = 100\,000$ K (central column, $\Gamma = 0.3$, $\chi = 0.02$) and $T = 50\,000$ K (right column, $\Gamma = 0.6$, $\chi = 0.06$) and to $r_s = 30$ (top row) and $r_s = 10$ (bottom row). $\Gamma$ and $\chi$ values correspond to $r_s = 10$. Points 2 and 3 present analytical results obtained according to [23, 45] respectively. Frequency and scaled dynamic conductivity is given in units of plasma frequency.

densities. The tails of the MMCF clearly show collective plasma oscillations. The decay time of the initial MMCF is strongly affected by variations of density and temperature. At a constant density the decay time is, at least, two times smaller for $T = 200\,000$ K compared to $T = 50\,000$ K. As it follows from figure 3, at constant $T$ the decay time increases with the rise of density. The physical reason is the tendency toward ordering of the charges.

### *3.3. Electrical conductivity*

Figure 4 presents the real part of the diagonal elements of the electrical conductivity tensor versus frequency, $\sigma(\omega)$, computed from the real part of the Fourier transform of the MMCF which characterizes the Ohmic absorption of electromagnetic energy. Collective plasma oscillations give the main contribution in the region of $\omega/\omega_p \sim 1$, where $\omega_p^2 = 4\pi n_e e^2/m_e$ is the electronic plasma frequency. Reliable numerical data in this region require very long dynamic trajectories. Their initial parts are presented in figure 3. The high-frequency tails of $\sigma(\omega)$ coincide with analytical Drude-like expressions for fully ionized hydrogen plasma obtained in [23, 44]. At low $\omega$ analytical estimations diverge which is the reason of the discrepancy with our numerical results. With increasing plasma density non-monotonic behavior of $\sigma(\omega)$ in the region of several plasma frequencies is observed which can be an indication of the transparency window (low-absorption coefficient) of the strongly coupled hydrogen plasma.

The agreement with Drude-like formulae for a weakly coupled plasma is due to the fact that the main contribution to the high-frequency region comes from the fast trajectories with high (virtual) energy. This means that interaction of electrons with each other and protons only weakly disturbs the high-frequency tail of $\sigma(\omega)$ with respect to an ideal plasma. Now let us consider the conductivity at very low plasma density. Figure 5 presents the MMCF and $\sigma(\omega)$ for $r_s = 43.2$ and temperatures from $T = 50\,000$ K up to $T = 10\,000$ K.

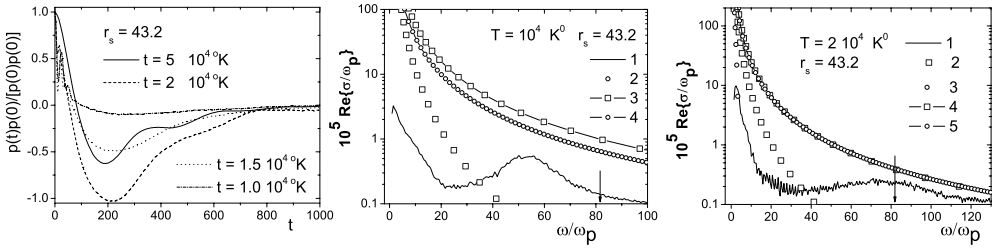


**Figure 5.** Typical MMCF in the canonical ensemble for $r_s = 43.2$ and four temperatures: $T = 50\,000$ K, $T = 20\,000$ K, $T = 15\,000$ K and $T = 10\,000$ K ($\Gamma = 0.7$, $\chi = 0.008$), time is presented in atomic units (left figure). Real part of the Fourier transform of MMCF (line 1) for density related to $r_s = 43.2$ and temperatures $T = 10\,000$ K (central figure) and $T = 20\,000$ K (right figure). Data points 2–5 present analytical results obtained according to [23, 44–46] respectively. The arrow corresponds to the condition $Ry = \hbar\omega$.

At $T \lesssim 50\,000$ K the plasma consists mainly of atoms. As a consequence the initial fast decay of the MMCF is modulated by high-frequency oscillations related to the ionization of atoms and motion of electrons inside the atoms. So the high-frequency tail of $\sigma(\omega)$ has a new maximum associated with the condition $Ry = \hbar\omega$. As it follows from figure 5 the position of this peak strongly depends on temperature and is shifted to lower frequency when temperature decreases. The probable physical reason is the ionization of hydrogen atoms which begins at lower frequencies at $T = 10\,000$ K because of the lowering of ionization potential. Analytical estimations for fully ionized plasma which are also presented in figure 5 give essentially larger values of $\sigma(\omega)$.

It can be seen from figures 4 and 5 that it is difficult to estimate the static electrical conductivity of a dense plasma because of strong oscillations of $\sigma(\omega)$ at low frequencies. To improve the accuracy it would be necessary to simulate much longer trajectories which requires significant computational efforts. We plan to perform such calculations and make a comparison with available experimental and theoretical data in the future.

## 4. Conclusion

We have used three approaches for the investigation of thermodynamic properties and electrical conductivity of dense hydrogen and deuterium plasma. Using two different methods of isentrope reconstruction from simulation results we obtained very good agreement with experimental data on quasi-isentropic compression of deuterium. We also applied the quantum dynamics approach to hydrogen plasma in a wide region of density and temperature. Calculating the MMCF we determined the dynamic electrical conductivity and compared the results with available theories. Our results show a strong dependence on the plasma coupling parameter. For low density and high temperature the numerical results agree well with the Drude approximation, while at higher values of the coupling parameter we observe a strong deviation of the frequency-dependent conductivity and permittivity from low-density and high-temperature approximations.

## Acknowledgments

The authors thank H Fehske for stimulating discussions and valuable notes. V Filinov acknowledges the hospitality of the of the Institut für Theoretische Physik und Astrophysik of the Christian-Albrechts-Universität zu Kiel.

## References


[1] Weir S T, Mitchell A C and Nellis W J 1996 *Phys. Rev. Lett.* **76** 1860–3
[2] Knudson M D, Hanson D L, Bailey J E, Hall C A, Assay J R and Deeney C 2004 *Phys. Rev.* B **69** 144209
[3] Da Silva L P *et al* 1997 *Phys. Rev. Lett.* **78** 483–6
[4] Boriskov G V, Bykov A I, Il'kaev R I, Selemir V D, Simakov G V, Trunin R F, Urlin V D, Shuikin A N and Nellis W J 2005 *Phys. Rev.* B **71** 092104
[5] Grishechkin S K *et al* 2004 *JETP Lett.* **76** 433–5
[6] Schlanges M, Bonitz M and Tschttschjan A 1995 *Contrib. Plasma Phys.* **35** 109
[7] Juranek H and Redmer R 2000 *J. Chem. Phys.* **112** 3780–6
[8] Fortov V E, Ternovoi V Ya, Zhernokletov M V, Mochalov M A, Mikhailov A L, Filimonov A S, Pyalling A A, Mintzev V B, Gryaznov V K and Iosilevskiĭ I L 2003 *JETP* **97** 259–78
[9] Kremp D, Schlanges M and Kraeft W-D 2005 *Quantum Statistics of Nonideal Plasmas* (Berlin: Springer)
[10] Kremp D, Bornath Th, Bonitz M and Schlanges M 1999 *Phys. Rev.* E **60** 4725
[11] Zubarev D N, Morozov V and Röpke G 1996 *Statistical Mechanics of Nonequilibrium Processes* (Berlin: Akademie Verlag)
[12] Bonev S A, Militzer B and Galli G 2004 *Phys. Rev.* B **69** 014101
[13] Holst B, Redmer R and Desjarlais M 2008 *Phys. Rev.* B **77** 184201
[14] Zamalin V M, Norman G E and Filinov V S 1977 *The Monte-Carlo Method in Statistical Thermodynamics* (Moscow: Nauka)
[15] Hansen J P and McDonald I R 1981 *Phys. Rev.* A **23** 2041
[16] Morozov I V and Norman G E 2005 *JETP Lett.* **100** 370
[17] Desjarlais M P 2003 *Phys. Rev.* B **68** 064204
[18] Filinov V S, Fehske H, Bonitz M, Fortov V E and Levashov P 2007 *Phys. Rev.* E **75** 036401
[19] Bezkrovniy V, Filinov V S, Kremp D, Bonitz M, Schlanges M, Kraeft W D, Levashov P R and Fortov V E 2004 *Phys. Rev.* E **70** 057401
[20] Johnson K J, Panagiotopoulos A Z and Gubbins K E 1994 *Mol. Phys.* **81** 717
[21] Liu L X and Su W L 2002 *Int. J. Quantum Chem.* **87** 1–11
[22] Filinov V S, Bonitz M, Ebeling W and Fortov V E 2001 *Plasma Phys. Control. Fusion* **43** 743
[23] Silin V P 1964 *ZheTF* **47** 2254
[24] Filinov V S 1996 *J. Mol. Phys.* **88** 1517–29
[25] Filinov V S, Lozovik Y, Filinov A, Zakharov E and Oparin A 1998 *Phys. Scr.* **58** 297–304
[26] Kelbg G 1963 *Ann. Phys.* **12** 219
[27] Filinov V S, Bonitz M and Fortov V E 2000 *JETP Lett.* **72** 245
[28] Filinov V S, Fortov V E, Bonitz M and Levashov P R 2001 *JETP Lett.* **74** 384
[29] Filinov A V, Bonitz M and Lozovik Y E 2001 *Phys. Rev. Lett.* **86** 3851
[30] Filinov V, Thomas P, Varga I, Meier T, Bonitz M, Fortov V and Koch S W 2002 *Phys. Rev.* B **65** 165124
[31] Filinov V, Medvedev Y and Kamskyi V 1995 *J. Mol. Phys.* **85** 717
[32] Widom B 1963 *J. Chem. Phys.* **39** 2808
[33] Arrieta E, Jedrzejek C and Marsh K N 1991 *J. Chem. Phys.* **95** 6838
[34] Zel'dovich Y B 1957 *JETP* **32** 1577
[35] Fortov V E and Krasnikov Y G 1970 *JETP* **59** 1645
[36] Levashov P R, Filinov V S, Botan A, Bonitz M and Fortov V E 2008 *J. Phys.: Conf. Ser.* **121** 012012
[37] Fortov V E *et al* 2007 *Phys. Rev. Lett.* **99** 185001
[38] Beule D, Ebeling W, Förster A, Juranek H, Nagel S, Redmer R and Röpke G *et al* 1999 *Phys. Rev.* B **59** 14177
[39] Scandolo S 2003 *Proc. Nat. Acad. Sci.* **100** 3051
[40] Ternovoi V Y, Filimonov A S, Fortov V E, Kvitov S V, Nikolaev D N and Pyalling A A 1999 *Physica* B **265** 6–11
[41] Fortov V E, Al'tshuler L V, Trunin R and Funtikov A I 2004 *Shock Waves and Extreme States of Matter* (New York: Springer)
[42] Datchi F, Loubeyre P and LeToullec R 2000 *Phys. Rev.* B **61** 6535
[43] Kerley G 1983 *Molecular-Based Study of Fluids* (Washington: American Chemical Society)
[44] Mihajlov A A, Djurić Z, Adamyan V M and Sakan N M 2001 *J. Phys. D: Appl. Phys.* **34** 3139
[45] Bornath T, Schlanges M, Hilse P, Kremp D and Bonitz M 2000 *Laser and Part. Beams* **18** 535
[46] Adamyan V M, Grubor D, Mihajlov A A, Sakan N M, Srecovic V A and Tkachenko I 2006 *J. Phys. A: Math. Gen.* **39** 4401